PAPER

Raman spectroscopy insights into the α- and δ-phases of formamidinium lead iodide (FAPbI₃)†

E. H. Driscoll, [iD] *[a] A. Orera, [iD] [b] P. A. Anderson,[a] M. L. Sanjuán[b] and P. R. Slater [iD] *[a]

Solar perovskites have received phenomenal attention and success over the past decade, due to their high power conversion efficiencies (PCE), ease of fabrication and low cost which has enabled the prospect of them being a real commercial contender to the traditional silicon technology. In one of the several developments on the archetypal MAPbI₃ perovskite absorber layer, FAPbI₃ was found to obtain a higher PCE, likely due to its more optimum band gap, with doping strategies focusing on the inclusion of MA^+/Cs^+ cations to avoid the unfavourable phase transformation to a photoinactive phase. To better understand the phase change from the photoactive cubic ($Pm\bar{3}m$) black (α) phase to the unwanted photoinactive ($P6_3/mmc$) yellow (δ) phase, we make use of variable temperature Raman spectroscopy to probe the molecular species and its relationship to the inorganic framework. We show for the first time there to be no Raman active modes for the α phase up to 4000 cm^{-1}, which can be correlated to the $Pm\bar{3}m$ cubic symmetry of that phase. Our detailed studies suggest that previous reports of the observation of Raman peaks for this phase are likely associated with degradation reactions from the localised laser exposure and the formation of Raman active lead oxide. In addition, we have identified water as a contributing factor to the transformation, and observed a corresponding signal in the Raman spectra, although confirmation of its exact role still remains inconclusive.

Introduction

In the past decade organic–inorganic lead halide perovskites – nominally referred to as solar perovskites – have gained significant attention in the photovoltaic community, due to their high efficiencies and their low fabrication costs. Initial developments began in 2009 when Miyasaka *et al.* demonstrated methylammonium lead halides (MAPbX₃; H₃CNH₃PbX₃) as visible light sensitizers, returning an efficiency of 3.9% for the iodide analogue in a device architecture.[1] At present the current power conversion efficiency (PCE) record stands at 25.5% for a single junction cell, whilst tandem silicon-perovskite cells have surpassed single junction silicon with a recorded efficiency of 29.1%.[2]

Although MAPbI₃ is considered to be the archetypal solar perovskite and has received considerable attention, this system suffers from poor moisture[3] and thermal stability.[4] MAPbI₃ is known to be sensitive to a humid environment resulting in the

irreversible formation of a dihydrate phase (MA₄PbI₆·2H₂O) in the dark, while in the presence of light, the degradation pathway results in the formation of PbI₂.[5,6] The exposure to oxygen and light has also been shown to cause degradation at a much greater rate than the moisture degradation pathway.[7] The oxygen and light degradation pathway is believed to proceed through the formation of a (photo-generated) superoxide (O_2^-) species which reacts with the organic component resulting in the formation of PbI₂, I₂ and methylamine (H₃CNH₂).[8] The iodide vacancies within the structure are believed to facilitate the degradation *via* the superoxide species.[9] Spectroscopy techniques, such as IR and Raman, have been employed multiple times to better understand the structural properties of this system, with the interaction of the organic component between the inorganic framework of MAPbI₃,[10–14] in addition to probing the mechanism[15,16] behind this material's significant performance and the degradation[17] stages.

The increased interest over the years in this field has seen rapid research and several developments on from MAPbI₃ to pursue greater efficiencies and increased (thermal) stability, and researchers have considered the analogues of formamidinium- (FA⁺; HC(NH₂)₂⁺)[18] and cesium-lead triodide[19] as alternatives. A range of compositions involving these two organic cations (MA⁺/FA⁺)[20–24] have also been investigated, in addition to further hybrids (FA⁺/Cs⁺)[23,25] or a mixture of all

[a]University of Birmingham, Edgbaston, Birmingham, B15 2TT, UK.
E-mail: ehd345@student.bham.ac.uk
[b]Instituto de Nanociencia y Materiales de Aragón (CSIC-Universidad de Zaragoza), c/ Pedro Cerbuna 12, 50009 Zaragoza, Spain

†Electronic supplementary information (ESI) available: Additional plotted Raman spectra consisting of: laser power adjustments, further black phase data and of the organic precursors. See DOI: 10.1039/d0dt04300a

three cations,[26,27] with the tuning of the bandgap with partial iodide substitution with bromide.[18,21,24,26,27] A common feature for all these developments is the inclusion of the formamidinium cation. As a stand-alone analogue, this system was found to achieve high PCE due its more optimal band gap[28] for single junction applications, and a higher thermal stability when compared to MAPbI$_3$. However the limitation in its potential relates to the unwanted phase transformation this material undergoes, from the photoactive black (cubic $Pm\bar{3}m$; α) phase to the unwanted photoinactive yellow (hexagonal $P6_3/mmc$; δ) phase, with the difference in structure relating to the connectivity of the PbI$_6$ octahedron bonding, where there is corner-sharing and face-sharing, respectively, for these two phases (Fig. 1). The yellow (δ) phase is nominally the most stable phase at room temperature, although the black (α) phase can be prepared during the synthesis and effectively quenched to room temperature. The δ phase can also be converted to the α phase on heating with the transition having been previously reported to be at 125 °C,[22,29] however, this transition has been found to take place as low as 77 °C [30] and up to 185 °C,[31] which has been attributed to kinetics of the technique in use and the selected synthesis ramp rate,[32] respectively. A wide variation also exists for the duration of the black phase stability, once formed, ranging from a matter of hours[23,33,34] up to days,[24,35–38] with the synthesis approach and the added nanoengineering templating[37,38] appearing to have an effect on stabilization.

The presence of water has been found to influence the morphology of the resulting FAPbI$_3$ perovskite, regardless of the gaseous environment in use, to produce porous metastable films.[39] Residual water trapped within the material upon formation has been found to result in the adsorption of protons and hydroxide ions at grain boundaries.[40] Although with this adsorption finding, the presence of water hasn't been cited as a direct link to the phase transformation, however the authors suggest this observation may relate to the transformation of these phases when the perovskite solar cells are exposed to ambient laboratory conditions.[40] With grain boundaries known to be high defect areas, the sample morphology in these films, would affect the level of packing and hence plausibly may account for the difference in phase stability.[32] Observations by Cordero et al. proposed the transformation to be driven by the highly hygroscopic character of the material and to be catalysed by humidity with additional extrinsic factors, such as grain boundaries (where considering compacted powders) influencing the instability.[32] The variations in the time elapsed for the phase transformation, in the different reports, is dependent on the experimental methods, samples and conditions. One observation to consider from this work is the ease of transformation of the α-FAPbI$_3$ upon grinding the sample.[32] This transformation likely highlights the need to store the samples under vacuum/in the absence of moisture, as the grinding of the sample results in the surface moisture to cause the transformation. However, like with many researchers, the use of thermogravimetric analysis has been inconclusive in terms of identifying the presence of water, as this signal is often undetected and the mass loss negligible[32,41] until the sample is heated high enough and decomposition occurs.

To add to the variance, original X-ray diffraction (XRD) studies reported the crystal system of the black (α) phase to be trigonal ($P3m1$),[22,29] whilst neutron diffraction has shown the symmetry to be cubic ($Pm\bar{3}m$).[41] The initial neutron diffraction by Weller et al. reported the FA$^+$ cation to be disordered over 12 possible sites,[41] with further work by Weber et al. investigating the resulting phase transition from cooling of the α-phase below room temperature.[42] The X-ray synchrotron data are also in agreement with the neutron studies.[42] And as a reiteration of previous statements, the authors state the cubic and hexagonal polymorphs interconvert rapidly depending on surrounding chemical environment.

Similarly to MAPbI$_3$, Raman spectroscopy has been used to investigate FAPbI$_3$ but to a lesser extent than XRD. The first report of Raman spectroscopy measurements to distinguish between the α- and δ-phases, to our knowledge, was by Han
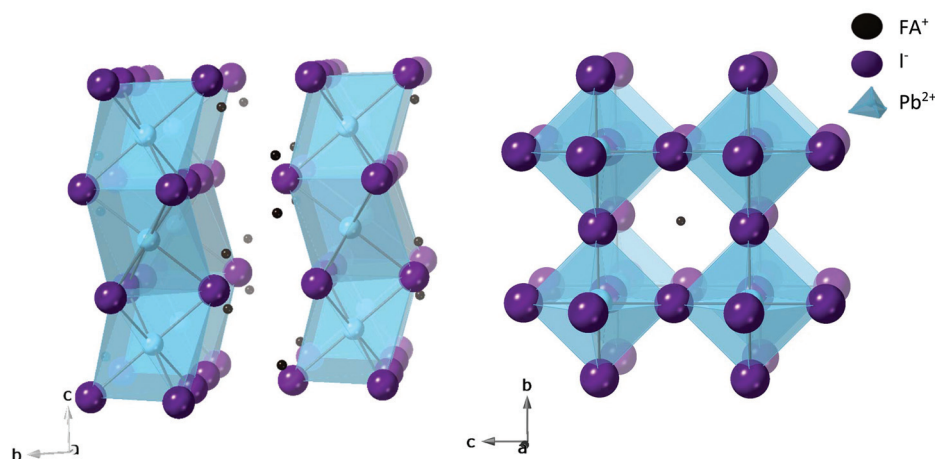

Fig. 1   Crystal structures of FAPbI$_3$ in the δ-phase (left) and α-phase (right).

et al. where the peak at lowest wavenumber was reported to be 135 cm^{-1} and 111 cm^{-1} in α- and δ-phases, respectively, with the data collected from 500 cm^{-1} down to 100 cm^{-1}.[31] However, our present work suggests that the band reported at 135 cm^{-1} in Han *et al.*[31] arises from the decomposition of the sample under laser exposure, thus could be due to PbO and not the perovskite material. A more recent study by Ruan *et al.*, considering FAPbX$_3$ (X = Cl, Br and I) probed the region of 1750 cm^{-1} down to 250 cm^{-1} and showed mainly the internal modes of the organic cations.[43] A study by Steele *et al.* made use of laser exposure of the FAPbI$_3$ material to transform *in situ* from the yellow to black phase.[44]

In this study, we make use of room and high temperature Raman for the δ-FAPbI$_3$ phase to investigate the molecular structural differences as the sample undergoes the phase transition to the black α-FAPbI$_3$ phase (Fig. 2). As a comparison, data for a room temperature stabilized α-FAPbI$_3$ sample have also been measured. Special attention has been paid to the possible presence of water within the structure.

Experimental

Solid state (SS)

Stoichiometric amounts of lead iodide (0.3642 g) and formamidinium iodide (0.1358 g) were dispensed, weighed and ground together, before being added to an alumina crucible for heating. The powders were heated to 150 °C for a total of 6 hours, with an intermittent grinding after each 3 hours interval. All resulting powders were stored in a desiccator.

Inverted temperature crystallization (ITC)

Based upon the original method by Saidaminov *et al.*,[45] the retrograde crystallization was implemented and adapted. Stoichiometric amounts of the solid precursors lead iodide (0.7283 g) and formamidinium iodide (0.2717 g) were dissolved into gamma-butyrolactone (GBL; 1.4872 g) to produce a 1.2 M solution. The resulting mixture was sonicated for a total of 6 minutes to ensure all of the lead precursor was dissolved. The solution was then filtered with 0.2 um Whatman PTFE filters producing a clear yellow solution, and the resulting filtrate added into a 10 mL round bottom flask. The round

bottom flask was stoppered and clamped into a pre-heated heating mantle set to 110 °C. To ensure thermal equilibrium, aluminium foil was used to cover the flask. The round bottom flask was heated for a total of 3 hours between 110–115 °C. As expected, multiple black crystals formed. The majority of the GBL solvent was then decanted before the crystals and remaining solvent were washed with *ca.* 3–5 mL of diethyl ether and air-dried in Buchner funnel and filter set up under vacuum. Diethyl ether was selected based upon Weller *et al.*'s[41] method of washing their FAPbI$_3$ crystals grown through a different synthesis route. The crystals were then collected and stored in a desiccator.

To validate the purity of the samples, from both methods, and our conclusions of the systems (without the implications of impurities obscuring our findings), powder X-ray diffraction data were recorded and are presented in this manuscript.

Instrumentation

Raman spectra collection. A DILOR XY spectrometer, with a CCD detector was used for the variable temperature and laser exposure studies. The 514.5 nm line of an Ar$^+$ laser was used with the power at the sample surface set at 2 mW, unless stated otherwise. A ×10 microscope objective lens was used both for excitation and light collection, with accumulation time of 1 min. The ×10 objective lens and the short accumulation time were chosen to minimise local heating effects. *In situ* variable temperature measurements were carried out in a Linkam TS1500 V stage with heating rates of 10 °C min^{-1} under air. The temperature was left to stabilise for several minutes before collecting each spectrum, to ensure that spectra were recorded at constant temperature.

For initial studies and measurements of the precursor samples *i.e.* PbO and PbI$_2$, a Renishaw inVia Raman microscope with a 532 nm laser line of 0.1% and 0.5% power respectively, was used to collect 20 accumulations with a 10 seconds exposure. For MAI and FAI (spectra found in the ESI†) the power rating used was 0.5% whilst retaining the other settings.

Powder X-ray diffraction (PXRD). X-ray powder diffraction data was collected on a Bruker D8/PANalytical Empyrean diffractometer (Cu source Kα).

Results and discussion

Methodology reasoning

Before evaluating the potential molecular differences and possible inclusion of water within the samples, stabilized samples of FAPbI$_3$ in the two different symmetries were required: cubic (*Pm3̄m*) and hexagonal (*P6$_3$/mmc*). Due to the ease of fabrication and reduced number of variables, we initially opted to prepare the perovskite *via* a SS route, however, this route requires thorough mixing of the precursors to avoid unwanted starting material impurities.

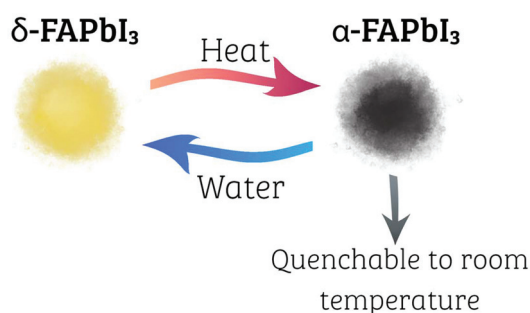The initial samples prepared *via* the SS route would nominally transform from the black α-phase to the δ-yellow phase

Fig. 2 Schematic showing how the phases investigated in this study relate with exposure to the different conditions.

over days. TGA measurements were conducted to assess any mass losses, such as possible water inclusion that is causing the unfavourable transformation. After the TGA measurement which involved a slow heating cycle up to 200 °C, the powder X-ray diffraction (PXRD) measurement showed the α-phase to be obtained afterwards. This sample, stored within a desiccator, remained within the meta-stable black phase with no degradation or phase-change after 8 months of storage (time interval from synthesis to Raman heating stage measurements). In addition to the lack of PbI_2 peaks in this pattern, the loss of formamidinium[29] which has been initially presumed to be causing the transformation can be ruled out. Regardless of lighting condition, by placing some of the black powder within a saturated water environment, the powder visibly changes to the yellow. The SS PXRD are shown in Fig. 3a–d.

In parallel to the SS synthesis route, an adapted ITC route was trialled. Upon synthesis of the crystals in the mother liquor, the crystals were observed to be black (as expected) but would start to transform to yellow upon removal of the GBL solvent and the consequential washing steps. The PXRD patterns after the ITC synthesis showed the $FAPbI_3$ to be compositional pure, but consisting of the α- and δ-phases.

The ITC route, although more complicated in set-up and with an increased number of variables, was elected as our primary synthesis method to produce multiple batches of phase pure hexagonal $FAPbI_3$. Ultimately this decision was due to avoiding unwanted starting materials which can occur *via* the SS route, such as PbI_2 from inconsistent mixing, which was observed on some occasions when producing additional batches to investigate, and hence could skew our conclusions. Although the crystals collected from the ITC route are a mixture of both phases (Fig. 3e), overnight a complete transformation to δ-phase occurred (Fig. 3f), and thus this ITC δ-$FAPbI_3$ was used in our transformation studies, followed by monitoring the Raman spectra changes upon heating. To compare with the ITC samples transformed from the δ to α, during these variable temperature Raman studies, we also examined at room temperature a stabilized SS α phase (described towards the latter end of this manuscript).

To deduce valid conclusions of the systems, it is imperative phase pure samples are be used. Therefore to confirm (phase) purity, PXRD patterns were collected and are presented in Fig. 3.

Given that Raman spectroscopy is a powerful technique to evaluate vibrational modes and molecular bonding within a structure, we decided to perform a detailed study with a view to gathering more information about the phase transformation. Raman spectroscopy is also unrivalled in phase identification and the detection of minor amount impurities. There are now more recent works regarding this technique and system, but initially Raman spectroscopy measurements had only been made use at low wavenumber[31] to differentiate between the two phases. In this study, we wanted to evaluate a greater range of spectra to better understand the molecular vibrations, in addition to consider any bands which would suggest water inclusion in the structure. We acknowledge at the time of writing this publication, a recent study by Ruan *et al.*[43] on the full spectra (excluding below 250 cm^{-1}, contrary to the earlier report which only focused on this lower region) has been published focusing on the FA internal modes, although the results aren't consistent with our findings, and the origin of the discrepancy is discussed below.

Symmetry considerations to deduce Raman modes

Before evaluating the results, we consider the Raman activity in the α- and δ-phases based upon their space groups (SGs) and thus, their resulting symmetry considerations. As is usual in compounds containing organic or quasi-molecular entities embedded in an inorganic framework, we separate the expected activity of the framework from that of the organic part and focus on the framework activity, which is expected to
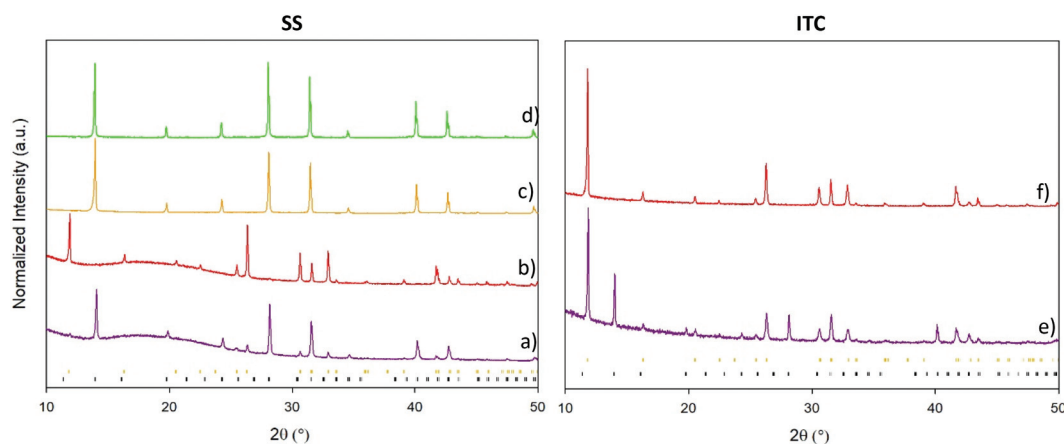

Fig. 3 Resulting PXRD patterns of samples prepared *via* SS (a–d) and ITC (e–f). SS: the sample after heating to 6 h at 150 °C (a), scanned 4 days later (b) and the resulting pattern after TGA conducted up to 200 °C (c). The same sample was found to retain the black photoactive phase 8 months later (d). Reference patterns of the black phase (black dashes – trigonal XRD pattern) and yellow phase (yellow dashes – hexagonal pattern) have been added for clarification. ITC: the as prepared crystals were scanned after synthesis and scanned a day later (f).

appear at low wavenumbers (≤300 cm^{-1}). In the undistorted perovskite structure of the α-phase SG $Pm\bar{3}m$, both Pb and I occupy sites with inversion symmetry and will therefore be Raman inactive. Regarding the organic part, its dynamic character (Weber *et al.*)[42] results in an isotropic and delocalised distribution which makes it also inactive.

Two different hexagonal SG have been proposed for the δ-phase: the non-centrosymmetric $P6_3mc$[29] and the centrosymmetric $P6_3/mmc$ one.[30,42] In the latter case Pb occupies the $2a$ Wyckoff site (with inversion symmetry, therefore Raman inactive) and I the 6 h site, yielding four (A_{1g}, E_{1g} and $2E_{2g}$) Raman active modes. In the non-centrosymmetric $P6_3mc$, on the other hand, seven modes ($3A_1 + 4E_1$) would be expected from the framework, both involving Pb and I.

Transformation of δ-FAPbI$_3$ phase with increasing temperature: 50–850 cm^{-1}

The room-temperature Raman spectrum of phase-pure δ-FAPbI$_3$ is shown in Fig. 4. The distinctive band of *ca.* 113 cm^{-1}, a representative feature of the yellow-phase,[31] is clearly identified. The same spectrum was homogeneously found throughout the sample, thus supporting that it does not arise from any impurity or second phase. Besides the intense 113 cm^{-1} band, three more bands (of low intensity in comparison to the 113 cm^{-1} one) are seen in this spectrum at ~63, 93 and 218 cm^{-1}. The number of observed modes in the low wavenumber range agrees more with the predictions from the SG $P6_3/mmc$, thus supporting a centrosymmetric structure for the δ phase at RT, in agreement with neutron diffraction results. The organic cation contributes modes at higher wavenumbers, as reported by Ruan *et al.*[43]

Although the δ-FAPbI$_3$ recorded spectrum (Fig. 4) looks very similar to the PbI$_2$ spectrum (Fig. 5), the δ-phase is confirmed as being present solely. If the sample contained PbI$_2$, the precursor would have been visible in the XRD patterns (which it is not) and we would see this peak continuously throughout the
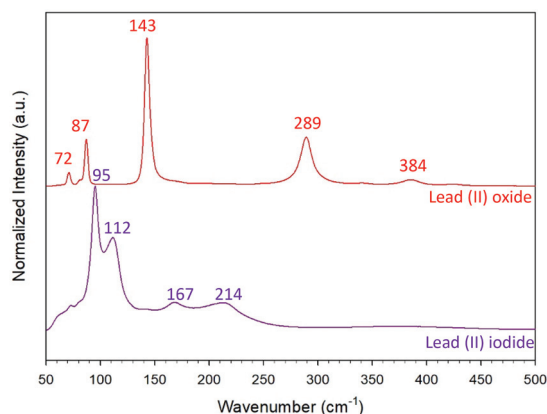

Fig. 5 Reference Raman spectra of lead(II) oxide (top) and lead(II) iodide (bottom).

different increasing temperature increments. The fact we see the signature peak at 113 cm^{-1} slowly decrease in intensity into the background confirms we are seeing the δ-phase.

The yellow (δ) sample prepared *via* the ITC was heated from room temperature (RT) to a maximum of 160 °C, above the reported transition temperature (Fig. 4). Before commencing our variable temperature study, we selected an appropriate laser power to allow for sufficient accumulations of the spectra to be collected which avoided degrading the surface nor to cause immeasurable changes (*i.e.* causing loss of water to the sample before data had finished being collected).

With increasing temperature, the signature band of the δ-phase at 113 cm^{-1} band becomes increasingly broader and noisier and is lost above 130 °C. At 135 °C up until 160 °C no clear Raman spectrum is observed, albeit a band is seen at *ca.* 142 cm^{-1} in the 150 °C spectrum (denoted with an asterisk) which is attributed to the decomposition of the sample to form lead oxide, facilitated by the sample conversion from δ to
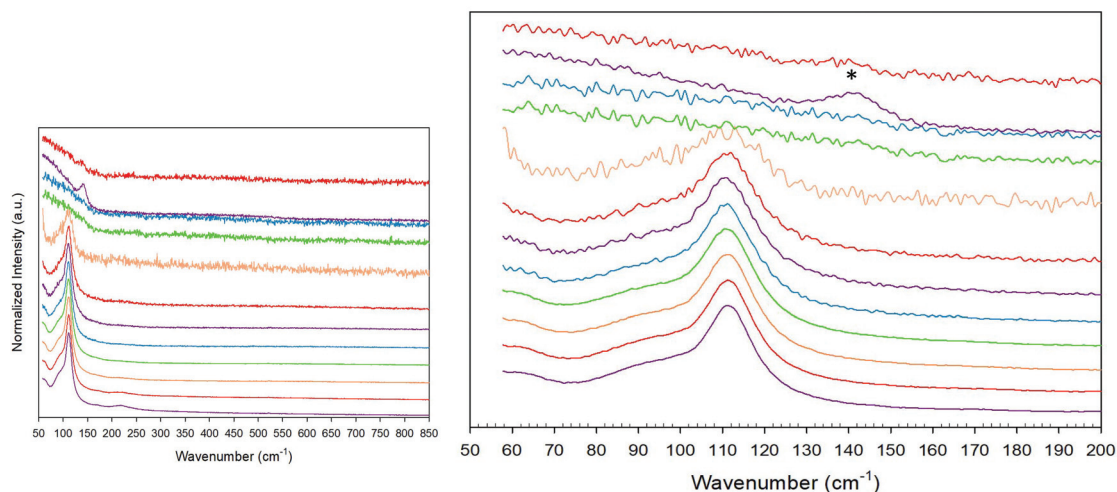

Fig. 4 Raman spectra of the yellow-phase of FAPbI$_3$ (crystals grown *via* the ITC route) as a function of temperature. The peak denoted with * relates to the decomposition of the sample to form lead oxide.
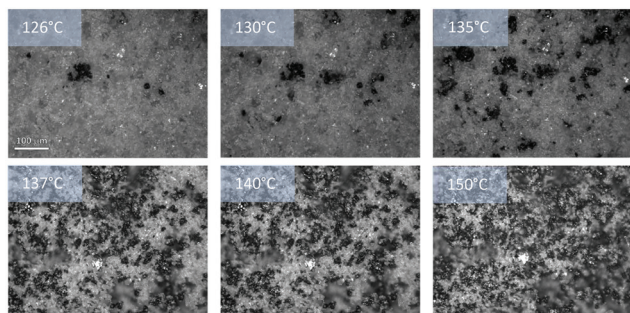
Fig. 6 Microscopy images of the sample whilst heating up to 160 °C in the low wavenumber region. Images were collected after 125 °C up to 150 °C.

α phases upon heating. The δ → α transition was confirmed by observation through the optical microscope in parallel with Raman data acquisition (Fig. 6). The collected images show, as expected, the transformation of the sample from the dullish grey (representative of the yellow phase) to the black crystallites of the α-phase. The transition temperature observed in this study at *ca.* 130 °C, matches previous reports,[22,29] however we'd like to indicate this transformation is likely the result of fast kinetics from the set ramping rate used. As a side note and a confirmation to previous reports[30] finding the transformation occurring as low as 77 °C, we heated a small amount of the yellow FAPbI$_3$ overnight at this set temperature, which resulted in the observation of a mixture of the yellow- and black-phases. Thus the variability of the transition temperature is the result of insufficient equilibrium and variability in kinetics. Because of the strong absorption in the black phase, laser irradiation may produce strong local heating, consequently resulting in decomposition. We note that, before measuring the spectrum at 160 °C, a new area of the sample was used, which is why this peak is much weaker in the 160 °C spectrum. To confirm that this band in the 150 °C spectra is associated with this decomposition product, reference patterns of lead oxide were measured (Fig. 5) showing agreement that this band is due to lead oxide. Using PXRD as a second confirmation technique of the presence of PbO was not possible in this study. Raman is a surface technique and degrading the sample would take a considerable amount of time, to produce enough sample for PXRD. In addition, the laser-induced degradation, when using a microscope, is a very local effect so that non-irradiated regions of the sample would not be decomposed, and thus the sample content might be very inhomogeneous. Thus, these results indicate that previous Raman spectra reported for the black (α) phase are likely the result of laser degradation producing signals from the degradation products and that the α-phase is inactive, as predicted by group theory.

A recent study by Ibaceta-Jaña *et al.* made use of DFT simulations to calculate the expected Raman modes of α-FAPbI$_3$, in addition to producing the crystals to compare their predictions to an experimental data set.[46] Their spectrum of the α-FAPbI$_3$

shows a peak at 114 cm^{-1} with a shoulder at 96 cm^{-1}, which match closely to the δ-FAPbI$_3$ spectrum recorded in this study. This suggests that Ibaceta-Jaña's spectrum may be due to the presence of some δ-phase coexisting with the α-phase, which has led to their misjudgement in the phase determination. Note that even a minor amount of a secondary phase may be predominant in the Raman spectrum when the main phase, as in this case, is Raman inactive and which has led to a false conclusion.

Transformation of δ-FAPbI$_3$ phase with increasing temperature: 1546 to 2239 cm^{-1}

To elucidate the role of water molecules in the α ↔ δ transformation we searched for bands that could be associated to water molecules. In this region we observed a decrease in the luminescence in the background with increasing temperature, in parallel to the δ → α phase transformation taking place, however, no bands are – once again – present.

Transformation of δ-FAPbI$_3$ phase with increasing temperature: 3217 to 3600 cm^{-1}

Considering the high wavenumber region of 3217 up to 3600 cm^{-1} (Fig. 7) a shallow band is present at *ca.* 3340 cm^{-1}, typical of water molecules, which disappears with increasing temperature. After these initial Raman measurements, the sample was returned to room temperature and left overnight in a saturated water environment, where the sample colour was observed to change from black to yellow. Re-measuring the sample on the instrument shows the re-appearance of this shallow band (Fig. 7). Ultimately, there is a competing process of heat exposure and moisture levels to the perovskites eventual phase. In a separate experiment, we trialled heating the δ-phase under a high humidity atmosphere (wet N$_2$) to 150 °C/0.5 C min^{-1}/0.5 h, where the resulting phase of the perovskite was found to be the α-phase. If in the case the level of humidity exposure outweighed the heating evaporation process, the yellow-phase is likely to be retained.
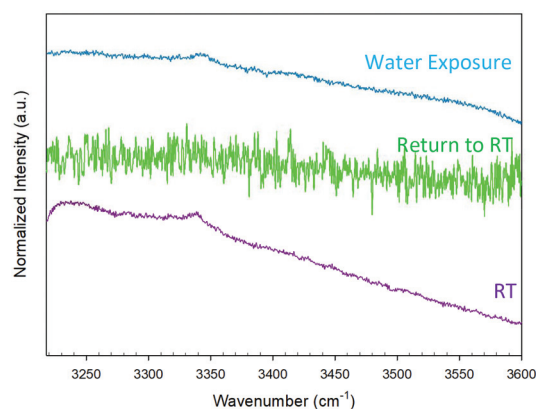

Fig. 7 Raman spectra of the yellow sample collected in the 3200−3600 wavenumber region from RT up to 130 °C before returning to RT and subjecting the sample to an overnight exposure to a saturated water environment, before re-measuring the sample (right).
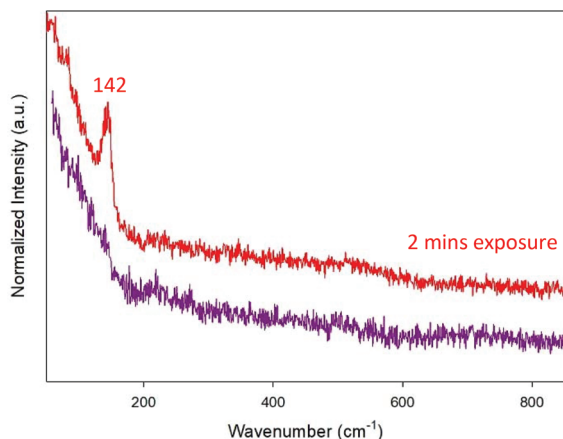
Fig. 8 Raman spectra of the black-phase of FAPbI$_3$ with a following measurement with 2 minutes, 2 mW laser exposure.

α-FAPbI$_3$ phase: Raman spectra comparison

As detailed above, from the heating stage measurements of the yellow (δ) phase of FAPbI$_3$ up to 135–140 °C, the sample visibly transforms into the black-phase where no bands are observed. To compare with the high temperature data, the stabilized room temperature black α-phase produced *via* the SS route was measured on the instrument at room temperature, with the collected spectra shown in Fig. 8. Similar to our previous high temperature observations, no Raman spectra was produced for this sample. Exposing the sample for 2 minutes under the 2 mW laser resulted in the appearance of a sharp peak at 142 cm^{-1}. This peak has commonly been associated with the spectra of the black phase, however, we regard it as a degradation product resulting from the increased laser exposure of the sample to form lead oxide. With neutron diffraction reporting the black phase to be of cubic ($Pm\bar{3}m$) symmetry, with dynamic disorder of the organic cations,[30,41] there should be no Raman active modes.[47] In the literature reports where the Raman spectra of the black phase has been reported, the results are thus likely to be from laser degradation products or the precursors themselves. A reference spectra of the organic cations iodides (MAI and FAI) commonly used in solar perovskites have been plotted and are presented in the ESI.†

Conclusions

Although FAPbI$_3$ has been thought to be an ideal candidate in place of the less thermal and moisture stable MAPbI$_3$, the drawback of the unfavourable phase transformation to the photoinactive yellow (δ) phase has rendered this undoped analogue unsuitable, regardless of the more optimum bandgap for single junction applications. With this system, there has been a lot of variance from the time of phase transformation elapsing from hours to days, in addition to the crystal symmetry proposed to be cubic over the initial proposal of trigonal symmetry, using neutron diffraction and single crystal X-ray diffraction, respectively.

To investigate the transformation of δ-($P6_3/mmc$) to α-($Pm\bar{3}m$) FAPbI$_3$, in addition to any long-range structural differences, Raman spectroscopy was selected to provide additional characterisation aspects, such as the presence of minor amounts of impurities or molecular species such as water and their role in the phase evolution, as well as to identify thermal-degradation products. Thus when probing samples with this technique it is paramount for samples to be high purity to avoid unwarranted conclusions.

Through heating the sample from room temperature to above the phase transition temperature – up to 160 °C, we have been able to reaffirm previous reports of the yellow phase spectra at low wavenumber being characterised mainly by a band at 113 cm^{-1} and in addition have shown the disappearance upon heating of a band at *ca.* 3340 cm^{-1} which we have attributed to the presence of water. A notable finding, contrary to previous reports, has been the demonstration of the absence of Raman bands for the black phase. On evaluating the literature concerning the black-phase structure to be that of undistorted cubic ($Pm\bar{3}m$) perovskite rather than trigonal as proposed with earlier X-ray diffraction reports, there should be no Raman-active modes, and this agrees with what we have observed. Thus, previous reports, which have proposed the low wavenumber band of *ca.* 140 cm^{-1} to be associated with the black phase have likely degraded their sample to form lead oxide from continual laser exposure, thus highlighting the need for careful studies in this area to preclude degradation products. We have identified water is a contributing factor to the transformation, however, have not yet conclusively identified its' role.

Abbreviations

PCE   Power conversion efficiencies
SG   Space group

Conflicts of interest

The authors declare no conflicts of interest for this body of work.

Acknowledgements

References

1 A. Kojima, K. Teshima, Y. Shirai and T. Miyasaka, *J. Am. Chem. Soc.*, 2009, **131**, 6050–6051.
2 NREL Efficiency Chart: Best research efficiencies chart, http://www.nrel.gov/pv/assets/images/efficiency_chart.jpg (accessed December 2020).

3 G. Niu, W. Li, F. Meng, L. Wang, H. Dong and Y. Qiu, *J. Mater. Chem. A*, 2014, **2**, 705–710.

4 B. Conings, J. Drijkoningen, N. Gauquelin, A. Babayigit, J. D'Haen, L. D'Olieslaeger, A. Ethirajan, J. Verbeeck, J. Manca, E. Mosconi, F. De Angelis and H. G. Boyen, *Adv. Energy Mater.*, 2015, **5**, 1–8.

5 S. N. Habisreutinger, T. Leijtens, G. E. Eperon, S. D. Stranks, R. J. Nicholas and H. J. Snaith, *Nano Lett.*, 2014, **14**, 5561–5568.

6 J. A. Christians, P. A. Miranda Herrera and P. V. Kamat, *J. Am. Chem. Soc.*, 2015, **137**, 1530–1538.

7 D. Bryant, N. Aristidou, S. Pont, I. Sanchez-Molina, T. Chotchunangatchaval, S. Wheeler, J. R. Durrant and S. A. Haque, *Energy Environ. Sci.*, 2016, **9**, 1655–1660.

8 N. Aristidou, I. Sanchez-Molina, T. Chotchuangchutchaval, M. Brown, L. Martinez, T. Rath and S. A. Haque, *Angew. Chem., Int. Ed.*, 2015, **54**, 8208–8212.

9 N. Aristidou, C. Eames, I. Sanchez-molina, X. Bu, J. Kosco, M. S. Islam and S. A. Haque, *Nat. Commun.*, 2017, **8**, 1–10.

10 C. Quarti, G. Grancini, E. Mosconi, P. Bruno, J. M. Ball, M. M. Lee, H. J. Snaith, A. Petrozza and F. De Angelis, *J. Phys. Chem. Lett.*, 2014, **5**, 279–284.

11 F. Brivio, J. M. Frost, J. M. Skelton, A. J. Jackson, O. J. Weber, M. T. Weller, A. R. Goñi, A. M. A. Leguy, P. R. F. Barnes and A. Walsh, *Phys. Rev. B: Condens. Matter Mater. Phys.*, 2015, **92**, 1–8.

12 A. A. Bakulin, O. Selig, H. J. Bakker, Y. L. A. Rezus, C. Müller, T. Glaser, R. Lovrincic, Z. Sun, Z. Chen, A. Walsh, J. M. Frost and T. L. C. Jansen, *J. Phys. Chem. Lett.*, 2015, **6**, 3663–3669.

13 L.-Q. Xie, T.-Y. Zhang, L. Chen, N. Guo, Y. Wang, G.-K. Liu, J.-R. Wang, J.-Z. Zhou, J.-W. Yan, Y.-X. Zhao, B.-W. Mao and Z.-Q. Tian, *Phys. Chem. Chem. Phys.*, 2016, **18**, 18112–18118.

14 R. G. Niemann, A. G. Kontos, D. Palles, E. I. Kamitsos, A. Kaltzoglou, F. Brivio, P. Falaras and P. J. Cameron, *J. Phys. Chem. C*, 2016, **120**, 2509–2519.

15 R. Gottesman, L. Gouda, B. S. Kalanoor, E. Haltzi, S. Tirosh, E. Rosh-Hodesh, Y. Tischler, A. Zaban, C. Quarti, E. Mosconi and F. De Angelis, *J. Phys. Chem. Lett.*, 2015, **6**, 2332–2338.

16 B.-W. Park, S. M. Jain, X. Zhang, A. Hagfeldt, G. Boschloo and T. Edvinsson, *ACS Nano*, 2015, **9**, 2088–2101.

17 M. Ledinský, P. Löper, B. Niesen, J. Holovský, S.-J. Moon, J. H. Yum, S. De Wolf, A. Fejfar and C. Ballif, *J. Phys. Chem. Lett.*, 2015, **6**, 401–406.

18 G. E. Eperon, S. D. Stranks, C. Menelaou, M. B. Johnston, L. M. Herz and H. J. Snaith, *Energy Environ. Sci.*, 2014, **7**, 982.

19 G. E. Eperon, G. M. Paternò, R. J. Sutton, A. Zampetti, A. A. Haghighirad, F. Cacialli and H. J. Snaith, *J. Mater. Chem. A*, 2015, **3**, 19688–19695.

20 N. Pellet, P. Gao, G. Gregori, T.-Y. Yang, M. K. Nazeeruddin, J. Maier and M. Grätzel, *Angew. Chem., Int. Ed.*, 2014, **53**, 3151–3157.

21 N. J. Jeon, J. H. Noh, W. S. Yang, Y. C. Kim, S. Ryu, J. Seo and S. Il Seok, *Nature*, 2015, **517**, 476–480.

22 A. Binek, F. C. Hanusch, P. Docampo and T. Bein, *J. Phys. Chem. Lett.*, 2015, **6**, 1249–1253.

23 J.-W. Lee, D.-H. Kim, H.-S. Kim, S.-W. Seo, S. M. Cho and N.-G. Park, *Adv. Energy Mater.*, 2015, **5**, 1–9.

24 X. Zheng, C. Wu, S. K. Jha, Z. Li, K. Zhu and S. Priya, *ACS Energy Lett.*, 2016, **1**, 1014–1020.

25 C. Yi, J. Luo, S. Meloni, A. Boziki, N. Ashari-Astani, C. Grätzel, S. M. Zakeeruddin, U. Röthlisberger and M. Grätzel, *Energy Environ. Sci.*, 2016, **9**, 656–662.

26 D. P. McMeekin, G. Sadoughi, W. Rehman, G. E. Eperon, M. Saliba, M. T. Horantner, A. Haghighirad, N. Sakai, L. Korte, B. Rech, M. B. Johnston, L. M. Herz and H. J. Snaith, *Science*, 2016, **351**, 151–155.

27 M. Saliba, T. Matsui, J.-Y. Seo, K. Domanski, J.-P. P. Correa-Baena, M. K. Nazeeruddin, S. M. Zakeeruddin, W. Tress, A. Abate, A. Hagfeldt and M. Grätzel, *Energy Environ. Sci.*, 2016, **9**, 1989–1997.

28 W. Shockley and H. J. Queisser, *J. Appl. Phys.*, 1961, **32**, 510–519.

29 C. C. Stoumpos, C. D. Malliakas and M. G. Kanatzidis, *Inorg. Chem.*, 2013, **52**, 9019–9038.

30 T. Chen, B. J. Foley, C. Park, C. M. Brown, L. W. Harriger, J. Lee, J. Ruff, M. Yoon, J. J. Choi and S.-H. Lee, *Sci. Adv.*, 2016, **2**, 1–6.

31 Q. Han, S.-H. Bae, P. Sun, Y.-T. Hsieh, Y. Yang, Y. S. Rim, H. Zhao, Q. Chen, W. Shi, G. Li and Y. Yang, *Adv. Mater.*, 2016, **28**, 2253–2258.

32 F. Cordero, F. Craciun, A. Trequattrini, A. Generosi, B. Paci, A. M. Paoletti and G. Pennesi, *J. Phys. Chem. Lett.*, 2019, **10**, 2463–2469.

33 Z. Li, M. Yang, J.-S. Park, S.-H. Wei, J. J. Berry and K. Zhu, *Chem. Mater.*, 2016, **28**, 284–292.

34 Y. Zhou, J. Kwun, H. F. Garces, S. Pang and N. P. Padture, *Chem. Commun.*, 2016, **52**, 7273–7275.

35 M. R. Leyden, M. V. Lee, S. R. Raga and Y. Qi, *J. Mater. Chem. A*, 2015, **3**, 16097–16103.

36 E. Smecca, Y. Numata, I. Deretzis, G. Pellegrino, S. Boninelli, T. Miyasaka, A. La Magna and A. Alberti, *Phys. Chem. Chem. Phys.*, 2016, **18**, 13413–13422.

37 X. Zhu, S. Zuo, Z. Yang, J. Feng, Z. Wang, X. Zhang, S. Priya, S. F. Liu and D. Yang, *ACS Appl. Mater. Interfaces*, 2018, **10**, 39802–39808.

38 L. Gu, D. Zhang, M. Kam, Q. Zhang, S. Poddar, Y. Fu, X. Mo and Z. Fan, *Nanoscale*, 2018, **10**, 15164–15172.

39 J. A. Aguiar, S. Wozny, N. R. Alkurd, M. Yang, L. Kovarik, T. G. Holesinger, M. Al-Jassim, K. Zhu, W. Zhou and J. J. Berry, *ACS Energy Lett.*, 2016, **1**, 155–161.

40 J. A. Aguiar, S. Wozny, T. G. Holesinger, T. Aoki, M. K. Patel, M. Yang, J. J. Berry, M. Al-Jassim, W. Zhou and K. Zhu, *Energy Environ. Sci.*, 2016, **9**, 2372–2382.

41 M. T. Weller, O. J. Weber, J. M. Frost and A. Walsh, *J. Phys. Chem. Lett.*, 2015, **6**, 3209–3212.

42 O. J. Weber, D. Ghosh, S. Gaines, P. F. Henry, A. B. Walker, M. S. Islam and M. T. Weller, *Chem. Mater.*, 2018, **30**, 3768–3778.

43 S. Ruan, D. P. McMeekin, R. Fan, N. A. S. Webster, H. Ebendorff-Heidepriem, Y.-B. Cheng, J. Lu, Y. Ruan and C. R. McNeill, *J. Phys. Chem. C*, 2020, **124**, 2265–2272.

44 J. A. Steele, H. Yuan, C. Y. X. Tan, M. Keshavarz, C. Steuwe, M. B. J. Roeffaers and J. Hofkens, *ACS Nano*, 2017, **11**, 8072–8083.

45 M. I. Saidaminov, A. L. Abdelhady, G. Maculan and O. M. Bakr, *Chem. Commun.*, 2015, **51**, 17658–17661.

46 J. Ibaceta-Jaña, R. Muydinov, P. Rosado, H. Mirhosseini, M. Chugh, O. Nazarenko, D. N. Dirin, D. Heinrich, M. R. Wagner, T. D. Kühne, B. Szyszka, M. V. Kovalenko and A. Hoffmann, *Phys. Chem. Chem. Phys.*, 2020, **22**, 5604–5614.

47 J. F. Shin, K. Joubel, D. C. Apperley and P. R. Slater, *J. Chem. Soc., Dalton Trans.*, 2012, **41**, 261–266.